

**Manuscript version: Published Version**

The version presented in WRAP is the published version (Version of Record).

**Persistent WRAP URL:**

<http://wrap.warwick.ac.uk/146651>

**How to cite:**

The repository item page linked to above, will contain details on accessing citation guidance from the publisher.

**Copyright and reuse:**

The Warwick Research Archive Portal (WRAP) makes this work by researchers of the University of Warwick available open access under the following conditions.

Copyright © and all moral rights to the version of the paper presented here belong to the individual author(s) and/or other copyright owners. To the extent reasonable and practicable the material made available in WRAP has been checked for eligibility before being made available.

Copies of full items can be used for personal research or study, educational, or not-for-profit purposes without prior permission or charge. Provided that the authors, title and full bibliographic details are credited, a hyperlink and/or URL is given for the original metadata page and the content is not changed in any way.

**Publisher's statement:**

Please refer to the repository item page, publisher's statement section, for further information.

For more information, please contact the WRAP Team at: [wrap@warwick.ac.uk](mailto:wrap@warwick.ac.uk)

# Continuous-Wave Magneto-Optical Determination of the Carrier Lifetime in Coherent $\text{Ge}_{1-x}\text{Sn}_x/\text{Ge}$ Heterostructures

Elisa Vitiello<sup>1,\*</sup>, Simone Rossi<sup>1,†</sup>, Christopher A. Broderick<sup>2,3</sup>, Giorgio Gravina,<sup>1</sup> Andrea Balocchi,<sup>4</sup> Xavier Marie,<sup>4</sup> Eoin P. O'Reilly<sup>2,3</sup>, Maksym Myronov<sup>5,‡</sup> and Fabio Pezzoli<sup>1</sup>

<sup>1</sup> *LNESS and Dipartimento di Scienza dei Materiali, Università degli Studi di Milano-Bicocca, Via R. Cozzi 55, 20125 Milan, Italy*

<sup>2</sup> *Tyndall National Institute, University College Cork, Lee Maltings, Dyke Parade, Cork T12 R5CP, Ireland*

<sup>3</sup> *Department of Physics, University College Cork, Cork T12 YN60, Ireland*

<sup>4</sup> *Université de Toulouse, INSA-CNRS-UPS, LPCNO, 135 Avenue de Rangueil, 31077 Toulouse, France*

<sup>5</sup> *Department of Physics, The University of Warwick, Coventry CV4 7AL, United Kingdom*



We present a magneto-optical study of the carrier dynamics in compressively strained  $\text{Ge}_{1-x}\text{Sn}_x$  films with Sn content up to 10% epitaxially grown on Ge on Si(001) virtual substrates. We leverage the Hanle effect under steady-state excitation to study the spin-dependent optical transitions in the presence of an external magnetic field. This allows us to obtain direct access to the dynamics of the optically induced carrier population. Our approach reveals that at cryogenic temperatures the effective lifetime of the photo-generated carriers in coherent  $\text{Ge}_{1-x}\text{Sn}_x$  is on the subnanosecond timescale. Supported by a model estimate of the radiative lifetime, our measurements indicate that carrier recombination is dominated by nonradiative processes. Our results thus provide central information to improve the fundamental understanding of carrier kinetics in this advanced direct-band-gap group-IV-material system. Such knowledge can be a stepping stone in the quest for the implementation of  $\text{Ge}_{1-x}\text{Sn}_x$ -based functional devices.

## I. INTRODUCTION

$\text{Ge}_{1-x}\text{Sn}_x$  binary alloys hold the promise of introducing advanced functionalities to the well-established and widespread Si technology [1–5]. The recent introduction of out-of-equilibrium growth techniques has been a key enabling factor to mitigate the long-standing problems associated with the low solubility of Sn in Ge and Si lattices and to tame defect injection induced by the sizeable lattice mismatch between these elements [6–8]. As a result, epitaxial Sn-containing alloys are now offering direct access to a wealth of intriguing phenomena, and are hence spurring a surge of interest.  $\text{Ge}_{1-x}\text{Sn}_x/\text{Ge}$  heteroepitaxial structures have recently shown tremendous improvements in lasing performances [9–12] and competitive photodetection efficiencies [13–15] in the technologically important mid-infrared wavelength range. These efforts are bringing  $\text{Ge}_{1-x}\text{Sn}_x$  heterostructures a step closer to a practical implementation as off-the-shelf photonic components. The intriguing application of strain and band-gap engineering, a well-established technology in group-IV heterostructures [16], could additionally result in the use of  $\text{Ge}_{1-x}\text{Sn}_x$

as a mobility booster in next-generation microelectronic devices [17,18]. Recently, the potential of  $\text{Ge}_{1-x}\text{Sn}_x$  heterostructures in fields such as spintronics and quantum technologies has been proposed [19].

Despite these extraordinary advancements, key properties of  $\text{Ge}_{1-x}\text{Sn}_x$  binary alloys relevant to device applications have largely remained unexplored. Notably, there is a critical lack of understanding of the mechanisms dominating carrier dynamics and nonradiative recombination, notwithstanding their crucial implications for transport and optical phenomena. Yet, such knowledge is pivotal also to facilitate future implementations of proposed photonic and electronic devices. Time-resolved methods applied to a vast range of experimental techniques, for example, absorption and photoluminescence (PL) spectroscopies are a primer to study the kinetics of the carriers. Although successful in addressing the spin physics of  $\text{Ge}_{0.95}\text{Sn}_{0.05}$  [19], time-resolved measurements has seldom been applied to  $\text{Ge}_{1-x}\text{Sn}_x$  alloys owing to the narrow band gap [20]. In addition to nontrivial structural problems associated with the spontaneous segregation of Sn, the band gap of  $\text{Ge}_{1-x}\text{Sn}_x$  typically lies in the shortwave or mid-infrared region. This has jeopardized a facile experimental achievement of adequate time and spectral resolutions, leading to a lack of insight regarding carrier dynamics in this emerging material system.

In this work, we introduce a radically different approach to provide such insight. We leverage steady-state optical spin orientation combined with a magneto-optical analysis of the radiative emission of ultrathin  $\text{Ge}_{1-x}\text{Sn}_x$  epitaxial layers. Specifically, we apply a technique so far overlooked in the context of group-IV materials—namely, the optical Hanle effect, in which the PL polarization is suppressed by an external magnetic field [21]. According to previous results for III-V compounds, the resulting polarization decay can be ascribed to the photogenerated-carrier dynamics [21]. Here we use the Hanle effect to reveal in  $\text{Ge}_{1-x}\text{Sn}_x$  the presence of an effective carrier lifetime in the subnanosecond regime without relying on demanding time-resolved techniques. We demonstrate the effectiveness of the present approach by exploring a wide Sn-content range spanning from 2% to 10%. Specifically, we use coherently grown  $\text{Ge}_{1-x}\text{Sn}_x$  films to avoid extrinsic decay pathways introduced by the nucleation of dislocations at the  $\text{Ge}_{1-x}\text{Sn}_x/\text{Ge}$  heterojunction. This study is eventually complemented and extended by preparing a second set of samples where the Sn content is kept constant while the dislocation density is precisely varied by changing the thickness of the epitaxial  $\text{Ge}_{1-x}\text{Sn}_x$  layer. This eventually enables us to gain access to nonradiative recombination induced by plastic strain relaxation, thus obtaining

central information—namely, the interface recombination velocity at the defective  $\text{Ge}_{1-x}\text{Sn}_x/\text{Ge}$  junction.

## II. RESULTS AND DISCUSSION

### A. Photoluminescence measurements

$\text{Ge}_{1-x}\text{Sn}_x/\text{Ge}/\text{Si}(001)$  heterostructures are grown with use of an ASM Epsilon 2000 industrial-type reduced-pressure-chemical-vapor-deposition (CVD) system. The epilayers of  $\text{Ge}_{1-x}\text{Sn}_x$  are deposited on a 100-mm-diameter Si(001) wafer via a relaxed Ge buffer with thickness approximately of 600 nm (see the schematic in the inset in Fig. 1). The structural properties of the samples are listed in Table I. All the  $\text{Ge}_{1-x}\text{Sn}_x$  films belonging to this first batch are under compressive strain and below the epilayer's critical thickness for the corresponding Sn content. The latter constraint is confirmed by means of asymmetrical reciprocal-space mapping using x-ray diffraction and is in line with previous literature reports [22–24]. A sample without the  $\text{Ge}_{1-x}\text{Sn}_x$  film is also measured as a reference. Continuous-wave PL experiments are performed at 10 K by exciting the samples with a Nd:YVO<sub>4</sub> laser at 1.165 eV. The spot diameter is about 50  $\mu\text{m}$  and the resulting optical power density is several kilowatts per square

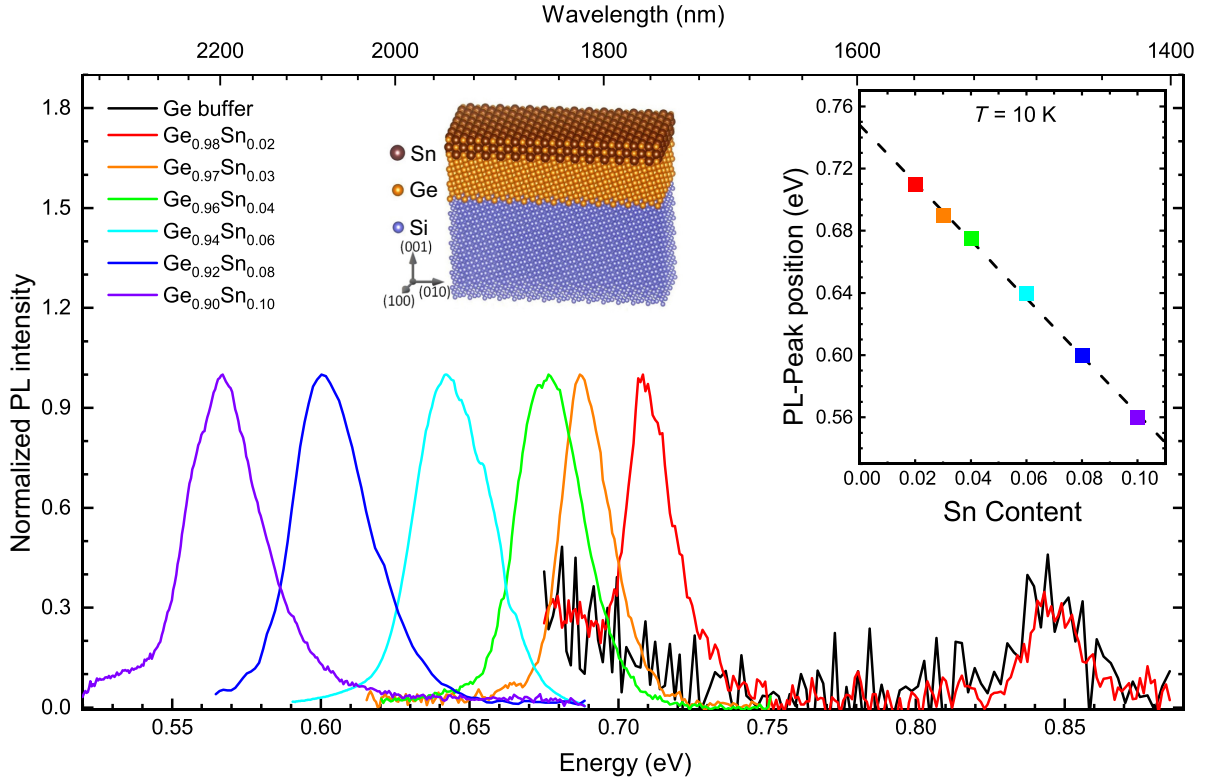


FIG. 1. PL spectra obtained at 10 K of  $\text{Ge}_{1-x}\text{Sn}_x$  with  $x$  ranging from 0 (Ge buffer, black curve) to 0.1 (violet curve). A sketch (not to scale) of the  $\text{Ge}_{1-x}\text{Sn}_x/\text{Ge}/\text{Si}$  heterostructure is presented: coherent  $\text{Ge}_{1-x}\text{Sn}_x$  layers with various Sn contents were grown on a 600-nm-thick Ge buffer layer deposited on a Si(001) substrate. The inset shows the energy of PL-peak maximum as a function of the Sn content. The dashed line is the linear fit.

TABLE I. Structural properties of  $\text{Ge}_{1-x}\text{Sn}_x$  layers grown coherently on the almost-relaxed Ge buffer, whose residual biaxial tensile strain stems from the difference in the thermal expansion coefficient with respect to the Si substrate. The thickness  $h$  of each layer is experimentally determined from x-ray-diffraction data.

Sn content (%)	$h$ (nm)
2	150
3	45
4	35
6	70
8	40
10	40

centimeter. The polarized PL is dispersed by a monochromator and coupled to an (In,Ga)As photodiode with a cutoff at approximately 0.5 eV

Figure 1 shows low-temperature PL spectra at 10 K of all the heterostructures investigated. The structural properties of  $\text{Ge}_{1-x}\text{Sn}_x$  epilayers are listed in Table I and sketched in the inset in Fig. 1. The tensile thermally strained Ge buffer layer shows a high-energy PL feature at about 0.85 eV (black line in Fig. 1), corresponding to direct-band-gap radiative recombination in Ge [25–27]. The addition of an ultrathin coherent  $\text{Ge}_{0.98}\text{Sn}_{0.02}$  cap layer to the Ge/Si epitaxial stack results in the emergence of a new prominent PL feature at about 0.71 eV (see the red spectrum in Fig. 1). Such a peak can be ascribed to band-to-band recombination events occurring in the topmost  $\text{Ge}_{0.98}\text{Sn}_{0.02}$  film. Increasing the Sn molar fraction  $x$  up to 10% results in a redshift of the PL-peak energy to 0.56 eV, in line with the Sn-induced band-gap reduction. The inset in Fig. 1 outlines this shrinkage of the band gap, which is determined by a combination of increasing Sn content in the  $\text{Ge}_{1-x}\text{Sn}_x$  alloy and subsequent increase of compressive strain in the epilayer, as reported previously [28,29]. The linear regression of the data (dashed line in Fig. 1) gives an intercept of about 0.75 eV at  $x = 0$  (i.e., elemental Ge). This value is consistent with the energy expected at low temperature for the optical transition through the fundamental indirect band gap of bulk Ge [30], thereby suggesting the prominence of the indirect-band-gap recombination in all the observed spectra of our coherent  $\text{Ge}_{1-x}\text{Sn}_x$  films. The emergence of the indirect PL in  $\text{Ge}_{1-x}\text{Sn}_x$  is also in line with the  $\Gamma$ - $L$  hybridization of the conduction-band edge pointed out by recent calculations [31,32].

Each PL peak is then studied through optical spin orientation. The circular polarization degree ( $\rho_{\text{circ}}$ ) of the PL is measured after circularly polarized laser excitation. Details regarding this technique can be found in previous work [25,33,34]. On average,  $\rho_{\text{circ}}$  is approximately 12% in our  $\text{Ge}_{1-x}\text{Sn}_x$  epitaxial films, demonstrating robust optical spin orientation. Since the spin relaxation time of

holes is expected to be significantly shorter than that associated with electrons, the latter primarily determines the experimentally accessible  $\rho_{\text{circ}}$  value [19,35,36].

## B. Hanle measurements and carrier lifetime

In the following, we introduce a magneto-optical investigation under continuous-wave excitation with the aim of elucidating the carrier dynamics in  $\text{Ge}_{1-x}\text{Sn}_x$ . Specifically, Hanle measurements are performed by sweeping the intensity of the magnetic field in a Voigt configuration; that is, along the direction orthogonal to the optically defined spin orientation [19]. Figure 2(a) shows that for all the samples,  $\rho_{\text{circ}}$  decays steadily with increasing strength of the external field. The data points are normalized to the zero-field value and henceforth mirrored to negative fields to better compare the expected Lorentzian line shape of the Hanle curves of the various  $\text{Ge}_{1-x}\text{Sn}_x$  layers [21,38].

The FWHM of the Hanle curve is related via the Bohr magneton  $\mu_B$  and the reduced Planck constant  $\hbar$  to the product  $\Pi$  of the effective electron Landé  $g$  factor and spin lifetime  $T_S$  as [21,38]

$$\Delta B = 2 \frac{\hbar}{g\mu_B T_S} = 2 \frac{\hbar}{\mu_b} \frac{1}{\Pi}. \quad (1)$$

Figure 2(a) notably demonstrates the surprising impact of Sn incorporation on the Hanle effect. A very weak magnetic flux density of about 20 mT is indeed sufficient to suppress the PL polarization of the  $\text{Ge}_{0.94}\text{Sn}_{0.06}$  layer [cyan curve in Fig. 2(a)], yielding the narrowest Hanle linewidth (i.e., the largest  $\Pi$  value of the samples investigated). The violet curve in Fig. 2(a) shows that the largest FWHM occurs for the epitaxial layer having the highest Sn molar fraction,  $x = 0.1$ . The  $\text{Ge}_{0.90}\text{Sn}_{0.10}$  film consequently possess the smallest  $\Pi$ . The nonmonotonic dependence of the extracted values of  $\Pi$  on the Sn molar fraction is shown in the inset in Fig. 2(a). Such intrinsic characteristics with a pronounced maximum at  $x = 0.06$  can be ultimately ascribed to the alloy-induced changes of both the Landé  $g$  factor and the spin lifetime.

It is worth noting, however, that all the coherent  $\text{Ge}_{1-x}\text{Sn}_x$  epilayers studied in this work possess a dominant indirect-band-gap character and a large built-in compressive strain. The optical transitions observed in our PL experiments thus allow us to gain access to the dynamics of spin-polarized electrons dwelling within the  $L$  valleys even in Sn-rich alloys. According to the only available data, which suggest a  $g$  value of 1.48 in  $\text{Ge}_{0.95}\text{Sn}_{0.05}$  [19], Sn incorporation in Ge is expected to smoothly decrease the  $g$  factor of conduction-band electrons from the pure-Ge value of approximately 1.6 [39–42]. This will result in a monotonic contribution to the  $\Pi$  dependence, suggesting that the bell-shaped behavior shown in the inset in Fig. 2(a) can be chiefly ascribed to the effect of alloying on the spin lifetime.

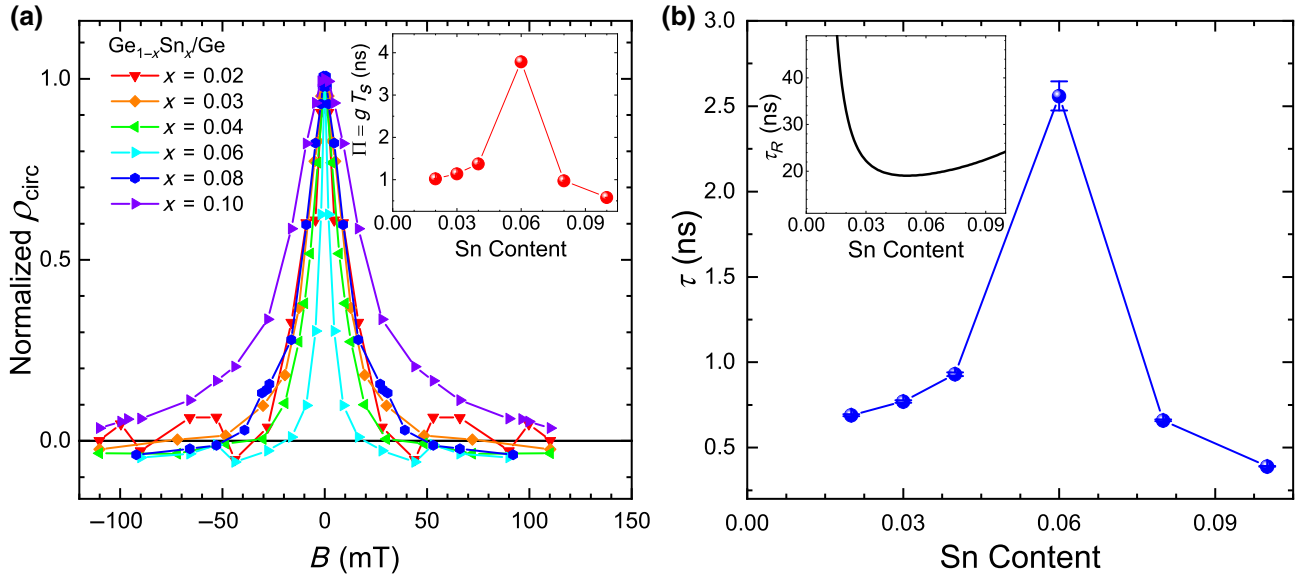


FIG. 2. (a) Low temperature (10 K) circular polarization degree  $\rho_{\text{circ}}$  as a function of transverse magnetic flux density (Hanle curve), normalized with respect the maximum  $\rho_{\text{circ}}$  for each  $\text{Ge}_{1-x}\text{Sn}_x$  layer. Data are mirrored to negative magnetic fields to better emphasize the Lorentzian character of the polarization decay. The inset shows the  $\Pi$  product ( $gT_S$ ), obtained from the FWHM of the Hanle curves, as a function of the Sn content. (b) Carrier lifetime  $\tau$  as a function of Sn content, obtained by assuming a constant  $g$  factor of 1.48 [19] and  $T_S \simeq \tau$ . The error bar is obtained by propagating the error of approximately 0.2 mT associated with measurement of the magnetic flux density. The inset shows the direct radiative lifetime  $\tau_R$  estimated via the model theoretical calculation outlined in Supplemental Material [37].

The latter is defined by the spin relaxation time  $\tau_S$  and the carrier lifetime  $\tau$  as  $T_S^{-1} = \tau^{-1} + \tau_S^{-1}$ . Nonetheless, the sizeable  $\rho_{\text{circ}}$  observed for all the samples under nonresonant excitation and in the absence of the external magnetic field implies that  $\tau_S > \tau$  and hence that  $T_S \simeq \tau$  [21]. This assumption was verified experimentally in a  $\text{Ge}_{0.95}\text{Sn}_{0.05}$  sample exhibiting spin relaxation time  $\tau_S \simeq 10$  ns and carrier lifetime  $\tau \simeq 2$  ns [19]. The fit of the Lorentzian Hanle curves in Fig. 2(a) therefore provides us with an estimate of the photogenerated-carrier lifetime without the need to rely on time-resolved measurements. Figure 2(b) shows the Sn-dependent  $\tau$  values derived from  $\Pi$  by assuming a constant  $g$  factor of 1.48 based on our recent experimental measurements [19]. The effective carrier lifetime is found to be on the order of hundreds of picoseconds and approaches 2 ns in the  $\text{Ge}_{0.94}\text{Sn}_{0.06}$  layer. Remarkably, this result compares well with the lifetime modeled by use of temperature-dependent PL characteristics by Wirths *et al.* [43], and is fully consistent with the value that was independently obtained by recent time-resolved PL investigations [19]. This further corroborates the effectiveness of our approach and supports the conclusion that our Hanle investigation can reliably yield information on the carrier kinetics in group-IV materials.

The measured carrier lifetime  $\tau$  corresponds to an effective lifetime for photogenerated carriers and encapsulates contributions from radiative ( $\tau_R$ ) and nonradiative ( $\tau_{\text{NR}}$ ) recombination processes:  $\tau^{-1} = \tau_R^{-1} + \tau_{\text{NR}}^{-1}$  [44]. Recent

analyses [31,32,45] have shown that the evolution of the  $\text{Ge}_{1-x}\text{Sn}_x$  band gap is driven by Sn-induced hybridization between the Ge  $\Gamma$ -point and  $L$ -point conduction-band-edge states. A direct band gap then emerges continuously with increasing Sn content, as the alloy conduction-band edge acquires increasing direct ( $\Gamma$ ) character. On this basis, it is expected that the radiative lifetime  $\tau_R$  decreases monotonically with increasing Sn content, as the alloy band gap acquires increasing direct character. To understand the measured trends in  $\tau$ , we perform a simple model estimate of the Sn-content-dependent  $\tau_R$ , on the basis of which we infer the role of nonradiative recombination. Our theoretical model—details of which are provided as Supplemental Material [37]—describes Sn-induced  $\Gamma$ - $L$  mixing using a model Hamiltonian parametrized via atomistic alloy-supercell electronic structure calculations. The lifetime  $\tau_R$  associated with direct radiative recombination is then computed as

$$\tau_R(x) = \frac{E_g(0)\tau_R(0)}{E_g(x)f_{\Gamma}(x)}, \quad (2)$$

where  $E_g(0)$  and  $E_g(x)$  are the direct band gaps of Ge and  $\text{Ge}_{1-x}\text{Sn}_x$ , respectively,  $f_{\Gamma}(x)$  is the Ge  $\Gamma$  character of the  $\text{Ge}_{1-x}\text{Sn}_x$  conduction-band edge, and  $\tau_R(0)$  is the radiative lifetime associated with the direct band gap in Ge. Using our theoretical model, we compute  $\tau_R(0) = 7.72$  ns, which is in good agreement with the value calculated



from first principles by Rödl *et al.* [46]. Our estimate of  $\tau_R$ , shown in the inset in Fig. 2(b), decreases with increasing Sn content, reaching a minimum value of 19.1 ns for  $x = 0.05$ . While this estimate ignores the impact of short-range substitutional alloy disorder on the band structure [32] and considers only zone-center transitions [46], these effects are expected to produce only minor quantitative changes to the computed  $\tau_R$ . This theoretical estimate does not consider phonon-assisted recombination. The simultaneous requirement for electron-hole recombination and phonon emission or absorption in such processes reduces the associated recombination rate, thereby increasing the associated lifetime. Therefore, our calculated  $\tau_R$  constitutes a lower bound on the radiative lifetime. On the basis that the calculated radiative lifetime is approximately 1 order of magnitude larger than the measured effective carrier lifetime, we conclude that carrier recombination in these samples is dominated by nonradiative recombination processes that occur sufficiently quickly to dominate the carrier kinetics.

Since the photogenerated excess carrier density is expected to be too low to give rise to significant Auger recombination [47], the likely scenario that explains the nonmonotonic variation of  $\tau$  with Sn content in Fig. 2(b) is related to the structural quality of the  $\text{Ge}_{1-x}\text{Sn}_x$  layers and to the challenge of minimizing crystal defects during the CVD of the epitaxial solid thin film. We thus recall that strong out-of-equilibrium conditions have to be applied to incorporate Sn into the Ge lattice; that is, low temperature (approximately 200–300 °C) and high growth rates to limit the surface diffusion of the adatoms. High Sn concentrations and strain values further decrease the Sn solubility [48,49]. This increases the tendency for Sn segregation and can result in the appearance of point defects and possible clustering of Sn. On the other hand, in the very-diluted-Sn regime the deposition temperature needs to be increased to approach the optimal growth temperature of elemental Ge. This eventually contributes to decrease the Sn incorporation, in spite of the Ge-rich environment and lower strain level of the target epitaxial layer. The competition of all these effects maximizes the structural quality of our coherent reduced-pressure-CVD  $\text{Ge}_{1-x}\text{Sn}_x$  films at intermediate Sn content  $x = 0.06$ , whose resulting superior optical properties manifest themselves through the lengthening of the effective carrier lifetime and give rise to the bell-shaped behavior shown in Fig. 2(b).

### C. Dislocation effects on effective carrier lifetime

Having addressed the carrier dynamics in coherently strained layers, in the following we extend the magneto-optical analysis to study partially relaxed materials. In so doing, we can gain insight into the nonradiative recombination pathways introduced by the nucleation of extended defects due to plastic strain relaxation. Here we consider

TABLE II.  $\text{Ge}_{0.92}\text{Sn}_{0.08}$  with different layer thickness  $h$ . The relaxation ( $R$ ) is experimentally determined from x-ray-diffraction data, and the linear dislocation density  $\delta$  is derived from the analysis of various TEM images. The strain relaxation of the 50-nm-thick sample is possibly below the experimental sensitivity, and thus the linear dislocation density of this sample is estimated according to the procedure described in Supplemental Material [37].

$h$ (nm)	$R$ (%)	$\delta$ ( $\mu\text{m}^{-1}$ )
40	0	0
50	0	0.2
60	0.6	0.59
80	6	2.28

a second set of samples having the same Sn molar fraction, namely,  $x = 0.08$ . The thickness of the  $\text{Ge}_{0.92}\text{Sn}_{0.08}$  epilayer is systematically varied across the critical thickness (i.e., between 40 and 80 nm). This investigated range is in good agreement with results on III-V materials [50] and the values reported at a comparable Sn content in Ref. [22]. This allows us to precisely tailor strain relaxation  $R$  and to suitably inject a well-controlled dislocation density. Table II summarizes the experimental data obtained by x-ray-diffraction and transmission-electron-microscopy (TEM) measurements, showing that  $R$  ranges from 0% to 6%, while the linear dislocation density  $\delta$  is between 0 and 2  $\mu\text{m}^{-1}$ . Figure 3(a) shows low-temperature PL spectra of the  $\text{Ge}_{0.92}\text{Sn}_{0.08}$  samples. We find that the PL intensity scales inversely with the epilayer thickness, so the thickest  $\text{Ge}_{0.92}\text{Sn}_{0.08}$  film demonstrates the weakest PL signal [51]. The suppression of the emission mimics the strain-relaxation process and reveals the introduction of nonradiative recombination pathways associated with the nucleation of dislocations at the interface between the  $\text{Ge}_{1-x}\text{Sn}_x$  layer and the underlying Ge buffer.

The Hanle curves reported in Fig. 3(b) clarify that by increase of the epilayer thickness  $h$  and thus the dislocation density  $\delta$ , the Hanle curve broadens, implying a reduction of the effective carrier lifetime  $\tau$ . The  $\tau$  values that are derived from the magneto-optical data are summarized in Fig. 3(c). The data points demonstrate the compelling link between the effective carrier lifetime and the layer thickness. Similar effects on the carrier lifetime have been observed in a strained III-V heterostructure [52].

We now elaborate further on this finding to provide a refined description of the kinetics that occurs in the presence of an increasing number of extended defects that can act as carrier sinks. First, we notice that recombination at the free surface provides a competing nonradiative channel. Yet, this has the same weight in the carrier dynamics of all the samples studied. The native oxide of the unpassivated surface cannot be modified by the mild strain relaxation of our epitaxial films. In addition, the laser penetration depth and the carrier diffusion guarantee a

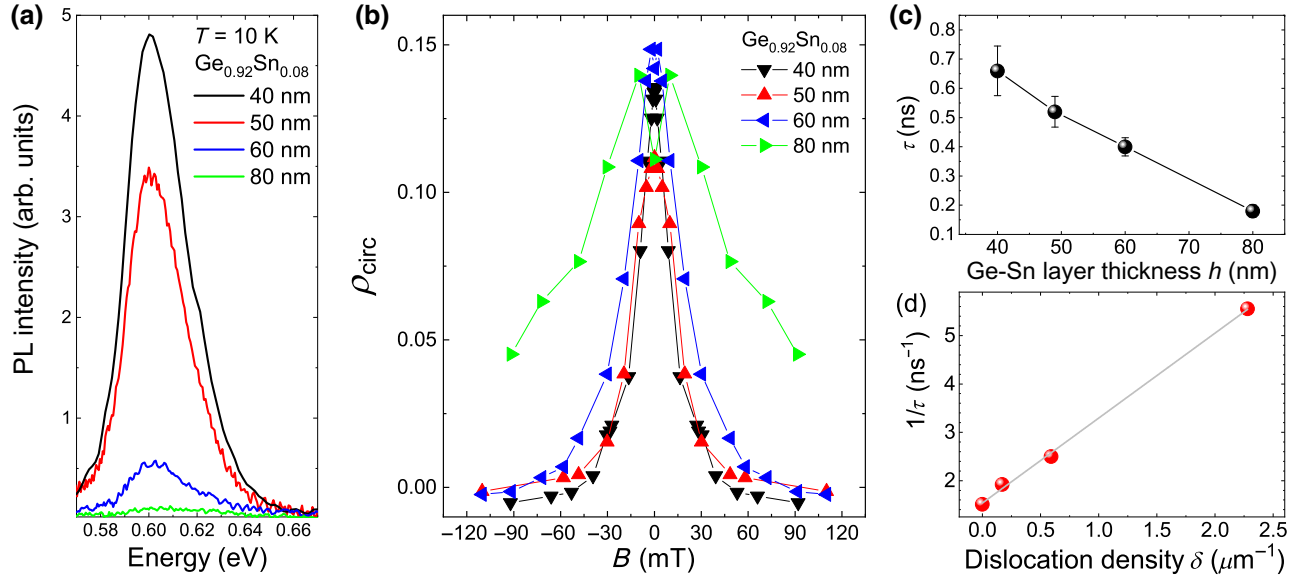


FIG. 3. (a) Low-temperature PL spectra and (b) Hanle curves of the  $\text{Ge}_{0.92}\text{Sn}_{0.08}$  layers with different thicknesses. Hanle data are mirrored at negative magnetic fields. (c) Carrier lifetime  $\tau$  as a function of layer thickness obtained from the Hanle decay curves. (d) Inverse of carrier lifetime as a function of the linear dislocation density. The linear fit shows an increase with a slope of  $(1.77 \pm 0.03) \times 10^5$  cm/s.

homogeneous distribution of the photogenerated carriers through the whole thickness of all the  $\text{Ge}_{0.92}\text{Sn}_{0.08}$  layers [53,54]. It is worth noticing that threading dislocations originating at the deeply buried Ge/Si buffer interface can pierce through the whole epitaxial stack, eventually emerging at the top free surface. However, these extended defects are expected to be equally present in all the samples investigated. As a result, changes in the nonradiative lifetime of the epitaxial films can be primarily ascribed to the emergence of recombination at the defective  $\text{Ge}_{1-x}\text{Sn}_x/\text{Ge}$  heterointerface.

In the framework of Shockley-Read-Hall statistics, the capture of minority carriers due to strain and Coulomb potentials dressing a dislocation line can be defined in terms of a recombination efficiency  $\sigma$  defined as [55,56]

$$\sigma = \frac{1}{\delta\tau}. \quad (3)$$

It follows that the recombination activity of dislocations can be interpreted as the probability that, within a mean lifetime, a photogenerated carrier funnels into one dislocation sink. The efficiency of this process can thus be inferred by a direct comparison between the experimentally accessible values of the carrier lifetime and the available dislocation sites.

We accordingly plot in Fig. 3(d) the measured carrier recombination rate  $\tau^{-1}$  as a function of the linear dislocation density as derived from the TEM analysis summarized in Table II (see Supplemental Material [37] for

more details). Figure 3(d) notably demonstrates a linear behavior. Such a result agrees well with the findings obtained in Si and Ge by Kurtz *et al.* [55,56]. The slope of the line that fits the data points shown in Fig. 3(d) provides us with a relevant experimental estimation of  $(1.77 \pm 0.03) \times 10^5$  cm/s for the recombination velocity at dislocations in  $\text{Ge}_{1-x}\text{Sn}_x$ . Remarkably, such a value is approximately 2 orders of magnitude larger than values previously reported for dislocated Si-rich SiGe/Si heterointerfaces [57,58] and between 2 and 10 times larger than values in junctions between Si and elemental Ge [59,60]. This should be carefully considered when one is optimizing  $\text{Ge}_{1-x}\text{Sn}_x$  heterostructures for future optoelectronic applications. Also, for fully strained  $\text{Ge}_{1-x}\text{Sn}_x$  epilayers, our characterization method based on magneto-optics is shown to be an accurate and reliable approach to improve and tailor the structural and optical quality of the material.

### III. CONCLUSIONS

We introduce an effective approach for the determination of the carrier lifetime, which has been largely overlooked in the context of group-IV materials. By taking advantage of well-developed steady-state magneto-optics, based on the Hanle effect, we unveil a subnanosecond lifetime for the photogenerated carriers in coherently strained  $\text{Ge}_{1-x}\text{Sn}_x$  epilayers. The investigation is performed up to a Sn content of 10%. Our findings suggest that the carrier kinetics is dominated by the presence of nonradiative defect-related recombination associated with imperfection

of the  $\text{Ge}_{1-x}\text{Sn}_x$  epitaxial material, arising due to the challenging epitaxy of  $\text{Ge}_{1-x}\text{Sn}_x$  by CVD at reduced pressure. By increasing the thickness of  $\text{Ge}_{1-x}\text{Sn}_x$  layers, we are able to promote and investigate the consequences of well-controlled plastic strain relaxation. We demonstrate the emergence of the parasitic nonradiative recombination associated with the concomitant nucleation of dislocations. Owing to the fast recombination velocity at the defective  $\text{Ge}_{1-x}\text{Sn}_x/\text{Ge}$  interface, the largest dislocation density corresponds to the shortest measured effective carrier lifetime.

Along with other applications, optical investigations based on the Hanle effect can also prove to be promising in resolving the critical thickness and the elastic-to-plastic relaxation onset in  $\text{Ge}_{1-x}\text{Sn}_x$  epitaxy. Our findings will inform fundamental investigations of the carrier dynamics in group-IV alloys and provide key information for the future design of  $\text{Ge}_{1-x}\text{Sn}_x$ -based devices, driving silicon photonic concepts and optoelectronic device design.

## ACKNOWLEDGMENTS

The authors thank L. Franzini for technical assistance. This work was supported by Science Foundation Ireland (project no. 15/IA/3082). C.A.B. acknowledges the support of the National University of Ireland Post-Doctoral Fellowship in the Sciences.

- [1] D. Liang and J. E. Bowers, Recent progress in lasers on silicon, *Nat. Phot.* **4**, 511 (2010).
- [2] Z. Fang, Q. Y. Chen, and C. Z. Zhao, A review of recent progress in lasers on silicon, *Opt. Laser Technol.* **46**, 103 (2013).
- [3] V. R. D'Costa, Y. Y. Fang, J. Tolle, J. Kouvetakis, and J. Menéndez, Tunable Optical gap at a Fixed Lattice Constant in group-IV Semiconductor Alloys, *Phys. Rev. Lett.* **102**, 107403 (2009).
- [4] R. A. Soref and L. Friedman, Direct-gap Ge/GeSn/Si and GeSn/Ge/Si heterostructures, *Superlattices Microstruc.* **14**, 189 (1993).
- [5] S. Assali, J. Nicolas, S. Mukherjee, A. Dijkstra, and O. Moutanabbir, Atomically uniform Sn-rich GeSn semiconductors with  $3.0 - 3.5 \mu\text{m}$  room-temperature optical emission, *Appl. Phys. Lett.* **112**, 251903 (2018).
- [6] B. Claffin, G. J. Grzybowski, M. E. Ware, S. Zollner, and A. M. Kiefer, Process for growth of group-IV alloys containing tin by remote plasma enhanced chemical vapor deposition, *Front. Mater.* **7**, 44 (2020).
- [7] S. Wirths, D. Buca, and S. Mantl, Si-Ge-Sn alloys: From growth to applications, *Prog. Cryst. Growth Charac. Mater.* **62**, 1 (2016).
- [8] J. Doherty, S. Biswas, E. Galluccio, C. A. Broderick, A. Garcia-Gil, R. Duffy, E. P. O'Reilly, and J. D. Holmes, Progress on germanium-tin nanoscale alloys, *Chem. Mater.* **32**, 4383 (2020).
- [9] Y. Zhou, W. Dou, W. Du, S. Ojo, H. Tran, S. A. Ghetmiri, J. Liu, G. Sun, R. Soref, J. Margetis, J. Tolle, B. Li, Z. Chen, M. Mortazavi, and S. Q. Yu, Optically pumped GeSn lasers operating at 270 K with broad waveguide structures on Si, *ACS Photon.* **6**, 1434 (2019).
- [10] D. Stange, S. Wirths, R. Geiger, C. Schulte-Braucks, B. Marzban, D. N. V. Driesch, G. Mussler, T. Zabel, T. Stoica, J. M. Hartmann, S. Mantl, Z. Ikonik, D. Grützmacher, H. Sigg, J. Witzens, and D. Buca, Optically pumped GeSn microdisk lasers on Si, *ACS Photon.* **3**, 1279 (2016).
- [11] S. Al-Kabi, S. A. Ghetmiri, J. Margetis, T. Pham, Y. Zhou, W. Dou, B. Collier, R. Quinde, W. Du, A. Mosleh, J. Liu, G. Sun, R. A. Soref, J. Tolle, B. Li, M. Mortazavi, H. A. Naseem, and S. Q. Yu, An optically pumped  $2.5 \mu\text{m}$  GeSn laser on Si operating at 110 K, *Appl. Phys. Lett.* **109**, 171105 (2016).
- [12] A. Elbaz, D. Buca, N. von den Driesch, K. Pantzas, G. Patriarche, N. Zerounian, E. Herth, X. Checoury, S. Sauvage, I. Sagnes, A. Foti, R. Ossikovski, J. M. Hartmann, F. Boeuf, Z. Ikonik, P. Boucaud, D. Grützmacher, and M. El Kurdi, Ultra-low-threshold continuous-wave and pulsed lasing in tensile-strained GeSn alloys, *Nat. Photon.* **14**, 375 (2020).
- [13] H. Tran, T. Pham, J. Margetis, Y. Zhou, W. Dou, P. C. Grant, J. M. Grant, S. Al-Kabi, G. Sun, R. A. Soref, J. Tolle, Y. H. Zhang, W. Du, B. Li, M. Mortazavi, and S. Q. Yu, Si-based GeSn photodetectors toward mid-infrared imaging applications, *ACS Photon.* **6**, 2807 (2019).
- [14] T. Pham, W. Du, H. Tran, J. Margetis, J. Tolle, G. Sun, R. A. Soref, H. A. Naseem, B. Li, and S.-Q. Yu, Systematic study of Si-based GeSn photodiodes with  $26 \mu\text{m}$  detector cutoff for short-wave infrared detection, *Opt. Express* **24**, 4519 (2016).
- [15] M. Oehme, K. Kostecky, K. Ye, S. Bechler, K. Ulbricht, M. Schmid, M. Kaschel, M. Gollhofer, R. Körner, W. Zhang, E. Kasper, and J. Schulze, GeSn-on-Si normal incidence photodetectors with bandwidths more than 40 GHz, *Opt. Express* **22**, 839 (2014).
- [16] S. De Cesari, E. Vitiello, A. Giorgioni, and F. Pezzoli, Progress towards spin-based light emission in group IV semiconductors, *Electronics* **6**, 19 (2017).
- [17] J. Zhou, G. Han, Q. Li, Y. Peng, X. Lu, C. Zhang, J. Zhang, Q. Q. Sun, D. W. Zhang, and Y. Hao, Ferroelectric  $\text{HfZrO}_x$  Ge and GeSn PMOSFETs with sub-60 mV/decade Sub-threshold Swing, Negligible Hysteresis, and Improved Ids, *IEDM*, 12.2.1 (2016).
- [18] M. Oehme, J. Werner, M. Gollhofer, M. Schmid, M. Kaschel, E. Kasper, and J. Schulze, Room-temperature electroluminescence from GeSn light-emitting pin diodes on Si, *IEEE Photonics Technol. Lett.* **23**, 1751 (2011).
- [19] S. De Cesari, A. Balocchi, E. Vitiello, P. Jahandar, E. Grilli, T. Amand, X. Marie, M. Myronov, and F. Pezzoli, Spin-coherent dynamics and carrier lifetime in strained  $\text{Ge}_{(1-x)}\text{Sn}_x$  semiconductors on silicon, *Phys. Rev. B* **99**, 035202 (2019).
- [20] B. Julsgaard, N. von den Driesch, P. Tidemand-Lichtenberg, C. Pedersen, Z. Ikonik, and D. Buca, Carrier lifetime of GeSn measured by spectrally resolved picosecond photoluminescence spectroscopy, *Photon. Res.* **8**, 788 (2020).



- [21] R. R. Parsons, Band-To-Band Optical Pumping in Solids and Polarized Photoluminescence, *Phys. Rev. Lett.* **23**, 1152 (1969).
- [22] F. Gencarelli, B. Vincent, J. Demeulemeester, A. Vantomme, A. Moussa, A. Franquet, A. Kumar, H. Bender, J. Meersschant, W. Vandervorst, R. Loo, M. Caymax, K. Temst, and M. Heyns, Crystalline properties and strain relaxation mechanism of CVD grown GeSn, *ECS J. Solid State Sci. Technol.* **2**, P134 (2013).
- [23] W. Wang, Q. Zhou, Y. Dong, E. S. Tok, and Y.-C. Yeo, Critical thickness for strain relaxation of  $\text{Ge}_{1-x}\text{Sn}_x$  semiconductors ( $x \leq 0.17$ ) grown by molecular beam epitaxy on Ge(001), *Appl. Phys. Lett.* **106**, 232106 (2015).
- [24] H. V. Stanchu, A. V. Kuchuk, Y. I. Mazur, J. Margetis, J. Tolle, S.-Q. Yu, and G. J. Salamo, Strain suppressed Sn incorporation in GeSn epitaxially grown on Ge/Si(001) substrate, *Appl. Phys. Lett.* **116**, 232101 (2020).
- [25] F. Pezzoli, L. Qing, A. Giorgioni, G. Isella, E. Grilli, M. Guzzi, and H. Dery, Spin and energy relaxation in germanium studied by spin-polarized direct-gap photoluminescence, *Phys. Rev. B* **88**, 045204 (2013).
- [26] S. De Cesari, R. Bergamaschini, E. Vitiello, A. Giorgioni, and F. Pezzoli, Optically reconfigurable polarized emission in germanium, *Sci. Rep.* **8**, 11119 (2018).
- [27] F. Pezzoli, A. Balocchi, E. Vitiello, T. Amand, and X. Marie, Optical orientation of electron spins and valence-band spectroscopy in germanium, *Phys. Rev. B* **91**, 201201(R) (2015).
- [28] K. Zelazna, M. P. Polak, P. Scharoch, J. Serafinczuk, M. Gladysiewicz, J. Misiewicz, J. Dekoster, and R. Kudrawiec, Electronic band structure of compressively strained  $\text{Ge}_{1-x}\text{Sn}_x$  with  $x = 0.11$  studied by contactless electroreflectance, *Appl. Phys. Lett.* **106**, 142102 (2015).
- [29] S. Al-Kabi, S. A. Ghetmiri, J. Margetis, W. Du, A. Mosleh, M. Alher, W. Dou, J. M. Grant, G. Sun, R. A. Soref, J. Tolle, B. Li, M. Mortazavi, H. A. Naseem, and S. Q. Yu, Optical characterization of Si-based  $\text{Ge}_{1-x}\text{Sn}_x$  alloys with Sn compositions up to 12%, *J. Electron. Mater.* **45**, 2133 (2016).
- [30] R. R. Lieten, K. Bustillo, T. Smets, E. Simoen, J. W. Ager III, E. E. Haller, and J.-P. Locquet, Photoluminescence of bulk germanium, *Phys. Rev. B* **86**, 35204 (2012).
- [31] E. J. O'Halloran, C. A. Broderick, D. S. Tanner, S. Schulz, and E. P. O'Reilly, Comparison of first principles and semi-empirical models of the structural and electronic properties of  $\text{Ge}_{1-x}\text{Sn}_x$  alloys, *Opt. Quantum Electron.* **51**, 314 (2019).
- [32] T. D. Eales, I. P. Marko, S. Schulz, E. O'Halloran, S. Ghetmiri, W. Du, Y. Zhou, S. Q. Yu, J. Margetis, J. Tolle, E. P. O'Reilly, and S. J. Sweeney,  $\text{Ge}_{1-x}\text{Sn}_x$  alloys: Consequences of band mixing effects for the evolution of the band gap  $\Gamma$ -character with Sn concentration, *Sci. Rep.* **9**, 14077 (2019).
- [33] F. Pezzoli, F. Bottegoni, D. Trivedi, F. Ciccacci, A. Giorgioni, P. Li, S. Cecchi, E. Grilli, Y. Song, M. Guzzi, H. Dery, and G. Isella, Optical Spin Injection and Spin Lifetime in Ge Heterostructures, *Phys. Rev. Lett.* **108**, 156603 (2012).
- [34] E. Vitiello, M. Virgilio, A. Giorgioni, J. Frigerio, E. Gatti, S. De Cesari, E. Bonera, E. Grilli, G. Isella, and F. Pezzoli, Spin-dependent direct gap emission in tensile-strained Ge films on Si substrates, *Phys. Rev. B* **92**, 201203(R) (2015).
- [35] E. J. Loren, J. Rioux, C. Lange, J. E. Sipe, H. M. van Driel, and A. L. Smirl, Hole spin relaxation and intervalley electron scattering in germanium, *Phys. Rev. B* **84**, 214307 (2011).
- [36] C. Lange, G. Isella, D. Chrastina, F. Pezzoli, N. S. Koester, R. Woscholski, and S. Chatterjee, Spin band-gap renormalization and hole spin dynamics in Ge/SiGe quantum wells, *Phys. Rev. B* **85**, 241303(R) (2012).
- [37] See Supplemental Material at <http://link.aps.org/supplemental/10.1103/PhysRevApplied.14.064068> for a detailed description of the theoretical model of the radiative lifetime and the thickness dependence of the dislocation density.
- [38] M. I. D'yakonov, and V. I. Perel, in *Optical Orientation*, edited by F. Meier, and B. P. Zakharchenya (North-Holland Physics Publishing, North Holland, Amsterdam, 1984).
- [39] A. Giorgioni, S. Paleari, S. Cecchi, E. Vitiello, E. Grilli, G. Isella, W. Jantsch, M. Fanciulli, and F. Pezzoli, Strong confinement-induced engineering of the  $g$  factor and lifetime of conduction electron spins in Ge quantum wells, *Nat. Commun.* **7**, 13886 (2016).
- [40] L. M. Roth and B. Lax,  $g$  Factor of Electrons in Germanium, *Phys. Rev. Lett.* **3**, 217 (1959).
- [41] C. Guite and V. Venkataraman, Measurement of Electron Spin Lifetime and Optical Orientation Efficiency in Germanium Using Electrical Detection of Radio Frequency Modulated Spin Polarization, *Phys. Rev. Lett.* **107**, 166603 (2011).
- [42] J. Lohrenz, T. Paschen, and M. Betz, Resonant spin amplification in intrinsic bulk germanium: Evidence for electron spin lifetimes exceeding 50 ns, *Phys. Rev. B* **89**, 121201(R) (2014).
- [43] S. Wirths, R. Geiger, N. Von Den Driesch, G. Mussler, T. Stoica, S. Mantl, Z. Ikonik, M. Luysberg, S. Chiussi, J. M. Hartmann, H. Sigg, J. Faist, D. Buca, and D. Grützmacher, Lasing in direct-bandgap GeSn alloy grown on Si, *Nat. Photon.* **9**, 88 (2015).
- [44] G. W. 't Hooft, W. A. J. A. van der Poel, L. W. Molenkamp, and C. T. Foxon, Giant oscillator strength of free excitons in GaAs, *Phys. Rev. B* **35**, 8281(R) (1987).
- [45] C. A. Broderick, M. D. Dunne, D. S. P. Tanner, A. C. Kirwan, E. J. O'Halloran, S. Schulz, and E. P. O'Reilly, in *Proc. 18th IEEE International Conference on Nanotechnology* (IEEE, 2018), p. 1.
- [46] C. Rödl, J. Furthmüller, J. R. Suckert, V. Armuzza, F. Bechstedt, and S. Botti, Accurate electronic and optical properties of hexagonal germanium for optoelectronic applications, *Phys. Rev. Mater.* **3**, 034602 (2019).
- [47] S. Dominici, H. Wen, F. Bertazzi, M. Goano, and E. Bellotti, Numerical study on the optical and carrier recombination processes in GeSn alloy for E-SWIR and MWIR optoelectronic applications, *Opt. Express* **24**, 26363 (2016).
- [48] V. H. Stanchu, V. A. Kuchuk, Y. I. Mazur, J. Margetis, J. Tolle, S.-Q. Yu, and G. J. Salamo, Strain suppressed Sn incorporation in GeSn epitaxially grown on Ge/Si(001) substrate, *Appl. Phys. Lett.* **116**, 232101 (2020).
- [49] M. Albani, S. Assali, M. A. Verheijen, S. Koelling, R. Bergamaschini, F. Pezzoli, E. P. Bakkers, and L. Miglio, Critical strain for Sn incorporation into spontaneously

- hr/>
- graded Ge/GeSn core/shell nanowires, [Nanoscale](#) **10**, 7250 (2018).
- [50] C. A. Broderick, S. Jin, I. P. Marko, K. Hild, P. Ludewig, Z. L. Bushell, W. Stolz, J. M. Rorison, E. P. O'Reilly, K. Volz, and S. J. Sweeney, GaAs<sub>1-x</sub>Bi<sub>x</sub>/GaN<sub>y</sub>As<sub>1-y</sub> type-II quantum wells: Novel strain-balanced heterostructures for GaAs-based near- and mid-infrared photonics, [Sci. Rep.](#) **7**, 46371 (2017).
- [51] F. Pezzoli, A. Giorgioni, D. Patchett, and M. Myronov, Temperature-dependent photoluminescence characteristics of GeSn epitaxial layers, [ACS Photon.](#) **3**, 2004 (2016).
- [52] T. Amand, X. Marie, B. Dareys, J. Barrau, M. Brousseau, D. J. Dunstan, J. Y. Emery, and L. Goldstein, Well-width dependence of the excitonic lifetime in strained III-V quantum wells, [J. Appl. Phys.](#) **72**, 2077 (1992).
- [53] H. Tran, W. Du, S. A. Ghetmiri, A. Mosleh, G. Sun, R. A. Soref, J. Margetis, J. Tolle, B. Li, H. A. Naseem, and S. Q. Yu, Systematic study of Ge<sub>1-x</sub>Sn<sub>x</sub> absorption coefficient and refractive index for the device applications of Si-based optoelectronics, [J. Appl. Phys.](#) **119**, 103106 (2016).
- [54] F. Pezzoli, F. Isa, G. Isella, V. C. Falub, T. Kreiliger, M. Salvalaglio, R. Bergamaschini, E. Grilli, M. Guzzi, H. Von Känel, and L. Miglio, Ge Crystals on Si Show Their Light, [Phys. Rev. Appl.](#) **1**, 044055 (2014).
- [55] A. D. Kurtz, S. A. Kulin, and B. L. Averbach, Effect of dislocations on minority carrier lifetime in semiconductors, [Phys. Rev.](#) **101**, 1285 (1956).
- [56] A. D. Kurtz, S. A. Kulin, and B. L. Averbach, Effects of growth rate on crystal perfection and lifetime in germanium, [J. of Appl. Phys.](#) **27**, 1287 (1956).
- [57] A. Trita, I. Cristiani, V. Degiorgio, D. Chrastina, and H. Von Känel, Measurement of carrier lifetime and interface recombination velocity in Si-Ge waveguides, [Appl. Phys. Lett.](#) **91**, 041112 (2007).
- [58] G. Grzybowski, R. Roucka, J. Mathews, L. Jiang, R. T. Beeler, J. Kouvetakis, and J. Menendez, Direct versus indirect optical recombination in Ge films grown on Si substrates, [Phys. Rev. B](#) **84**, 205307 (2011).
- [59] R. Geiger, J. Frigerio, M. J. Süess, D. Chrastina, G. Isella, R. Spolenak, J. Faist, and H. Sigg, Excess carrier lifetimes in Ge layers on Si, [Appl. Phys. Lett.](#) **104**, 062106 (2014).
- [60] S. A. Srinivasan, M. Pantouvaki, P. Verheyen, G. Lepage, P. Absil, J. Van Campenhout, and D. Van Thourhout, Extraction of carrier lifetime in Ge waveguides using pump probe spectroscopy, [Appl. Phys. Lett.](#) **108**, 211101 (2016).